IEEE Access
Multidisciplinary | Rapid Review | Open Access Journal

Received December 14, 2017, accepted January 28, 2018, date of publication February 12, 2018, date of current version March 15, 2018.

Digital Object Identifier 10.1109/ACCESS.2018.2805264

High-Frequency Acoustic Estimation of Time-Varying Underwater Sparse Channels Using Multiple Sources and Receivers Operated Simultaneously

SAMAR KADDOURI[1], (Member, IEEE), PIERRE-PHILIPPE J. BEAUJEAN[1], (Member, IEEE), AND PIERRE-JEAN BOUVET[2], (Member, IEEE)

[1]Department of Ocean and Mechanical Engineering, Florida Atlantic University, Dania Beach, FL 33004, USA
[2]Department of Embedded Systems, Acoustic and Communications, ISEN Brest YNCREA Ouest, 29200 Brest, France

Corresponding author: Pierre-Philippe J. Beaujean (pbeaujea@fau.edu)

ABSTRACT In this paper, the authors propose a robust underwater acoustic field estimation of the time-varying channel impulse response for simultaneous transmissions using multiple sources and multiple receivers [multi-in multi-out (MIMO)] that closely follows the rapidly time-varying nature of the underwater acoustic channel. The presented algorithm outlines a time-varying underwater channel estimation method based on the channel sparsity characteristic. The method uses the MIMO P-iterative greedy orthogonal matching pursuit algorithm and takes advantage of the sparsity of the underwater acoustic channel. This technique is compared to a trended least square estimation method presented by the authors in a previous publication. Both techniques are demonstrated in a fully controlled environment, using simulated and experimental data, and the results in each case show a significant improvement in the estimation of the channel impulse response.

INDEX TERMS Underwater channel estimation.

I. INTRODUCTION

The short-range and medium-range (up to 1 nautical mile) shallow water underwater acoustic channels have rapidly changing time-varying channel impulse response [1]. The acoustic multipath is both pronounced and time-dependent, which causes severe signal distortions between sources and receivers. This issue applies to any bistatic sonar application. For example, the data transmission rate of underwater acoustic communication systems is severely limited due to the time-varying multipath [2], [3].

Gaining knowledge of the time-varying channel impulse response is highly beneficial in most underwater acoustic applications, especially if this information is available for spatially distributed sources and receivers. A well known example in shallow waters is ocean acoustic tomography (OAT) [4]–[6] at mid-frequency (around 2.5 kHz) using a set of sources and receivers, that was introduced by Munk and Wunsh [7] as a remote-sensing technique for large-scale monitoring of the ocean interior using sound. Taking advantage of multipath propagation to further improve the medium coverage, OAT relies on the identification and tracking of echoes' arrivals, and it uses the time variations of each echo to estimate the ocean variability. A time-delay mapping of the underwater channel impulse response is then used in the estimation of the medium physical properties, such as sound speed variations or currents [8]–[10]. To identify and use an echo in the tomography process, it is essential to track this echo over time and to unambiguously associate this echo with with a specific path [11]. As with most application of underwater acoustics, OAT has mainly relied on using low-to-mid frequency sounds. However, ambient noise at frequencies over 200 kHz is due to thermal agitation. Such noise is mostly stationary has well-known statistical properties. By contrast, lower frequency noise is often non-stationary, highly colored and includes bursts. As a result, filtering and de-noising routines are more effective at high-frequencies [12].

In addition, the underwater channel's time variability results in large Doppler spreading and this phenomenon can dramatically affect the performance of traditional channel estimation routines, such as the LS estimation

approach [13], [14]. Therefore, for such diverse applications as shallow water acoustic tomography, underwater acoustic communications, underwater acoustic source tracking (among others), there is a clear benefit to develop a robust algorithm to track the time-evolving fluctuations of the underwater acoustic environment at very-high frequencies and in a MIMO configuration.

As a result, channel estimation techniques are of great interest in underwater acoustic communications [15]–[24]. For example, in [15], the sparsity of the channel delay Doppler spread function is exploited to estimate a time-varying channel in a single source-single receiver transmission at a carrier frequency of 18 kHz. However, in general, the research remains mostly confined to applications with frequencies lower than 30 kHz mostly using a single source [15]–[18], [20]–[22]. On the other hand, existing references on high frequency underwater communications [19], [24] do not deals with MIMO channel estimation.

This paper propose a robust channel estimation technique for simultaneous transmissions at very-high frequency using multiple sources and multiple receivers that closely follows the rapidly time-varying nature of the underwater channel. The proposed approach is to exploit the underwater sparsity characteristics using an MIMO orthogonal matching pursuit algorithm (MIMO-OMP) technique, which isolates the most significant echoes and efficiently tracks the quick time changes in the channel impulse response. For this analysis, the underwater acoustic (UWA) channel is characterized by a limited number of dominant echoes and is considered as a sparse channel, a feature used by the iterative orthogonal matching pursuit (OMP) algorithm.

The OMP algorithm is commonly used for estimation of static UWA channels as it outperforms conventional least squares methods in that case, i.e. when only the time of arrivals is estimated. One major difference in this paper is that the channel impulse response is dynamic, thus it is estimated both as a function of time and time delay. This method is compared to a previously proposed approach that combines a trend extraction algorithm to the LS technique that is called the trended-LS method [13]. The proposed MIMO-OMP method would be a powerful tool for Doppler spread measurement and UWA channel equalization at very high frequencies. We again want to stress that the channel estimation techniques in the UWA systems have been limited to applications with frequencies lower than 30 kHz and have not been tested to perform correctly at much higher frequencies. In addition, while the OMP algorithm for MIMO systems has been well studied in terrestrial communication channels [25]–[27], it has not been considered before in the underwater acoustic channel. The novelty of this work is twofold: First, it studies and analyzes the performance of the OMP algorithm applied to MIMO underwater acoustic communications at very high-frequencies (around 300 kHz). Second, it tests and compares a newly developed technique, the trended-LS algorithm, to the MIMO-OMP and the LS techniques also in the context of MIMO systems at very high-frequencies.

This paper is organized as follows: Section II presents a background on acoustic communications and focuses on the multipath aspect of the acoustic signal transmission.

Section III outlines the proposed algorithm for estimating high frequency multipath MIMO channels. For this purpose, the UWA channel sparsity is used to estimate and isolate each echo in every sub-channel of the MIMO channel impulse response (CIR). In Section IV, the proposed MIMO-OMP channel estimation technique is evaluated and compared against two different methods using simulated channels: the LS method and the trended-LS method. We analyze the performance of each algorithm according to the relative root mean error square (noted RMSE through the text) produced between the modeled channels and their resulting estimations. The performance is studied as a function of two parameters: increasing noise level and increasing number of iterations. In Section V, the proposed algorithm's performance is tested in actual MIMO experiments with two sources and two receivers. Finally, Section VI summarizes the main results and conclusions of this work.

II. MIMO TIME-VARYING CHANNEL ESTIMATION OVERVIEW

In a MIMO transmission, for an unknown channel $\mathbf{h}_{ij}[n]$ of length L_c sampled at time n between a transmitter i and a receiver j, the relationship between a received signal $\mathbf{r}_j$ received on the j^{th} receiver and a transmitted signal $\mathbf{s}_i$ sent on the i^{th} transmitter is formulated as:

$$\mathbf{r}_j[n] = \mathbf{S}[n]\mathbf{h}_j[n] + \mathbf{w}_j[n] \tag{1}$$

where $\mathbf{h}_j[n] = \left[\mathbf{h}_{1j}^T[n] \cdots \mathbf{h}_{N_t j}^T[n]\right]^T$ is the column vector of the channel impulse response coefficients between all transmitters and the j^{th} receiver, $\mathbf{S}[n]$ is the augmented matrix formed based on $\mathbf{s}_i[n]$ for $i \in [1, N_t]$. We assume that the signals $\mathbf{s}_i$ for all i and $\mathbf{w}_j$ for all j are uncorrelated and that $\mathbf{S}$ is known. Here, the CIR $\mathbf{h}_j$ is the unknown, whereas the transmitted signal serves as an aid for the estimation and are known as "reference signals" or pilots. The objective is now to calculate an estimate $\hat{\mathbf{h}}_j$ of $\mathbf{h}_j$ of highest possible accuracy, based on a measurement $\mathbf{r}_j$.

Since the CIR is typically non-stationary for underwater channels with relatively long durations, any channel estimation method is typically applied to shorter time-gated, overlapping sections of the source signal (as shown in Figure 1), resulting in a time-varying estimation of the channel. If the sections overlap by only one time sample, we obtain an estimate of the CIR at every time index n. This CIR estimation is performed over a total of N_w time windows of equal length L_w. Sequential time windows are time-shifted by $L_{ov} = L_w(1 - O_w)$ elements, where O_w is the overlap ratio between sequential time windows. Every time window starts at time index $n = kL_{ov}$ where $k \in [0, N_w - 1]$ is the window index.

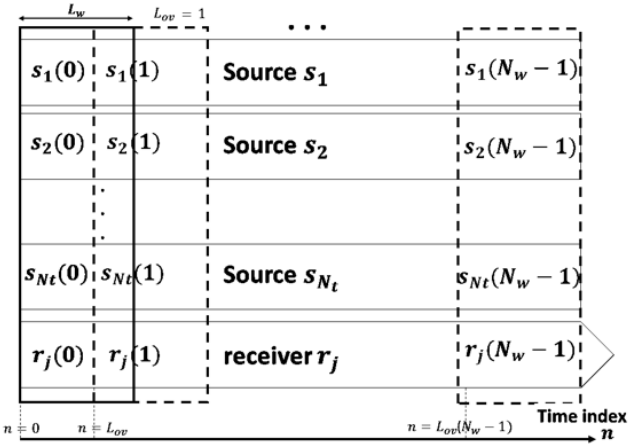

FIGURE 1. Channel estimation diagram.

If L_c is the length of the estimated CIR with $L_c \leq L_w$, the augmented source signal matrix $\mathbf{S}_i[n]$ of size $(L_w - L_c + 1) \times L_c$ is represented as:

$$\mathbf{S}_i[n] = \begin{bmatrix} s_i(n+L_c-1) & s_i(n+L_c-2) & \cdots \\ s_i(n+L_c) & s_i(n+L_c-1) & \cdots \\ s_i(n+L_c+1) & s_i(n+L_c) & \cdots \\ \vdots & \vdots & \vdots \\ s_i(n+L_w-1) & s_i(n+L_w-2) & \cdots \end{bmatrix}. \quad (2)$$

$\mathbf{S}[n]$ is of size $(L_w - L_c + 1) \times N_t L_c$ and is the concatenation of the $\mathbf{S}_i$ matrices as:

$$\mathbf{S}[n] = \begin{bmatrix} \mathbf{S}_1[n] & \mathbf{S}_2[n] & \cdots & \mathbf{S}_{N_t}[n] \end{bmatrix}. \quad (3)$$

$\mathbf{r}_j$ represents the received signal of size $(L_w - L_c + 1) \times 1$ such that:

$$\mathbf{r}_j[n] = \begin{bmatrix} r_j[n+L_c-1] & r_j[n+L_c] & \cdots & r_j[n+L_w-1] \end{bmatrix}^T. \quad (4)$$

$\hat{\mathbf{h}}_j[n]$ represents the CIR estimate of size $N_t L_c \times 1$ at sampling time n:

$$\hat{\mathbf{h}}_j[n] = \begin{bmatrix} \hat{\mathbf{h}}_j[n,0] & \hat{\mathbf{h}}_j[n,1] & \cdots & \hat{\mathbf{h}}_j[n,L_c-1] \end{bmatrix}^T. \quad (5)$$

where $\hat{\mathbf{h}}_j[n,l] = \begin{bmatrix} \hat{h}_{1j}[n,l] & \ldots & \hat{h}_{N_t j}[n,l] \end{bmatrix}$. On the other hand, $\mathbf{w}_j[n]$ represents the noise array of size $(L_w - L_c + 1) \times 1$ at sampling times n and combines the ambient noise of the channel and the uncorrelated echoes from prior parts of the transmitted sequence. For each echo, the estimated CIR coefficients are stored in a complex form. In order to easily analyze the channel time variations in the following sections, we define a new vector $\hat{\mathbf{h}}_{ij}[l]$ of size $N_w \times 1$ to containing the time variation of the l^{th} estimated echo, such that:

$$\hat{\mathbf{h}}_{ij}[l] = \begin{bmatrix} \hat{h}_{ij}[0,l] & \hat{h}_{ij}[L_{ov},l] & \cdots & \hat{h}_{ij}[(N_w-1)L_{ov},l] \end{bmatrix}. \quad (6)$$

One of the most common channel estimation techniques is the LS technique. It is a very powerful tool to estimate time-varying CIR. Its application on a high-frequency transmission in underwater channels has already been investigated by Real *et al.* [28]. An extension of this method, called trended-LS, added a trend extraction algorithm to the traditional LS method [13]. While the values for the relative Root-Mean-Square Error (RMSE) achieved between the estimated channel and the real channel were encouraging, they could clearly be improved.

III. EXPLOITING SPARSITY

A. OVERVIEW

Channels with a large delay spread but with few echoes are described as having a sparse impulse response and are encountered in a number of different applications. Underwater acoustic channels exhibit a similar response [29]. Therefore, many channel estimation techniques exploit the sparsity of the UWA channel using different algorithms, such as basis pursuit (BP) [30]–[32], matching pursuit (MP) [33]–[35] and orthogonal matching pursuit (OMP) [15], [36]. In [33], an estimate of a single-input single-output (SISO) channel obtained using a basic MP algorithm is shown to be more accurate than an LS estimate of a channel where each of the tap values will in general be nonzero. In [34], this MP estimate is compared to a thresholded variant of the LS channel (ThLS) estimate. The MP estimate is shown to be computationally much simpler to implement and requires a shorter known sequence to form an accurate channel estimate. Rao [37] uses a sparse LS estimate (SpLS) that is obtained by re-estimating the ThLS nonzero taps.

The accuracy of each of the techniques in [29], [33], and [34] is compared in [35] and their effectiveness quantified by considering their use in the UWA channel equalization process. It is seen that there is no distinguishable difference in performance between the MP and SpLS-based estimators, while the complexity of implementing the MP algorithm is much lower than that of the SpLS algorithm. In addition, the MP estimate is more robust to drops in the SNR than LS estimates for a same training sequence length.

In [36], the OMP algorithm for SISO channel estimation is used. Not only does it eliminate the convergence problem in the MP algorithm based on re-selection of the basis vectors, but the re-selection process also produces more accurate channel estimates. The performance of UWA channel equalizers using the MP and OMP algorithms indicates that the OMP outperforms the MP, with a comparable computational complexity.

In the following sections, the OMP algorithm is applied to a time-varying MIMO transmission at very high-frequencies, and its performance is evaluated and compared against both the LS and the trended-LS methods.

B. ORTHOGONAL MATCHING PURSUIT

The OMP algorithm is an iterative process with P iterations that searches for the closest matching projection of the received signal onto a dictionary comprised of transmitted signal data vectors. We first find the column in the matrix which is best aligned with the received vector, then

the projection of this vector along this direction is removed and a residual vector is obtained. The algorithm proceeds by sequentially choosing the column which best matches the residual vector until some termination criterion is met. The OMP algorithm also eliminates the convergence problem of the simple MP algorithm [32], [38] caused by the possible re-selection of the basis vectors in the dictionary matrix. Another advantage of the OMP algorithm is that we only need half the number of pilots required in the LS estimation algorithm [39], thereby improving the channel capacity. The pseudo-code presented in algorithm 1 summarizes the main steps of the OMP applied to a MIMO system, and is named the MIMO-OMP algorithm.

Algorithm 1 MIMO-OMP Algorithm

1: **procedure** OMP($\mathbf{r}_j[n]$, $\mathbf{S}[n]$)
2: **Initialize:**
$\mathbf{g}_0 \leftarrow \mathbf{r}_j[n]$, P total number of iterations,
$\mathbf{A}_0 = [\,]$, $I_0 = \{\}$, iteration counter p = 1.
3: **Identify:**
- Find $c_p = \underset{k\in[1,N_tL_c],k\notin I_p}{\operatorname{argmax}} |\mathbf{e}_k^T \mathbf{S}^H[n]\mathbf{g}_{p-1}|^2$
with $i = \lceil c_p/L_c \rceil$, $l = c_p - (i-1)L_c - 1$ and
$\mathbf{e}_k$ is the unit column vector with 1 at the k^{th}
element and 0 elsewhere.
4: **Compute and Construct:**
- Compute $\hat{h}_{ij}[n, l] = \frac{\mathbf{e}_{c_p}^T \mathbf{S}^H[n]\mathbf{g}_{p-1}}{|\mathbf{e}_{c_p}^T \mathbf{S}[n]|^2}$.
- Set $\mathbf{A}_p = \left[\mathbf{A}_{p-1} \quad \mathbf{e}_{c_p}^T \mathbf{S}[n]\right]$, $I_p = I_{p-1} \cup c_p$.
5: **Update:**
- Compute
$\mathbf{g}_p = \left(\mathbf{I}_{L_w-L_c+1} - \mathbf{A}_p(\mathbf{A}_p^H\mathbf{A}_p)^{-1}\mathbf{A}_p^H\right)\mathbf{r}_j[n]$,
where $\mathbf{I}_N$ is the identity matrix of size
$N \times N$.
- If p = P stop, otherwise set p = p+1 and
repeat from 3.
6: **end procedure**

IV. SIMULATION

In the following section, we evaluate the proposed MIMO channel estimation routines and analyze their performance when applied first to time-invariant then to time-varying modeled channels. The MIMO modeled setup consists of two sources s_1 and s_2 and two receivers r_1 and r_2. In an effort to keep the paper concise, we focus the analysis on the estimated CIR $h_{12}(\tau)$ between source s_1 and receiver r_2 in the time-invariant case, and on the direct path of the estimated CIR $h_{12}(t, \tau)$ in the time-varying case.

A. MODELED MIMO CHANNELS

The channels used to generate the simulated received signals were modeled using a 3D stochastic model presented by Kaddouri *et al.* [39], [40]. The model combines a method of images in an enclosed 3-D environment, originally presented in [41] and the Rayleigh stochastic model. The simulated setup is shown in Figure 2 and the parameters of the simulated channel are shown in Table 1.

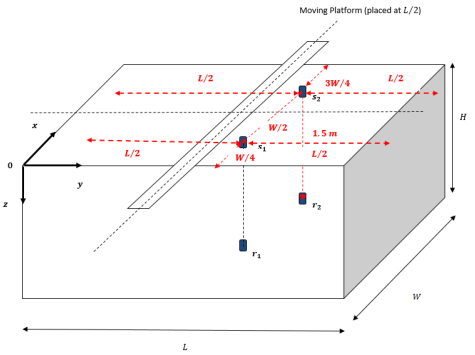

FIGURE 2. Modeled MIMO setup.

TABLE 1. MIMO modeled channel simulation parameters.

Parameters	Symbol	Value	
Duct Length	L	9.1	[m]
Duct Width	W	7.6	[m]
Duct Height	H	3.8	[m]
Source 1 Location	src	(W/4,L/2,0.1)	[m]
Source 2 Location	src	(3W/4,L/2,0.1)	[m]
Receiver 1 Location	rcv	(W/4, L/2,1.6)	[m]
Receiver 2 Location	rcv	(3W/4, L/2,1.6)	[m]
Sound Speed in water	c_w	1529.28	[m/s]
Sampling Frequency	f_s	75	[kHz]
Center Frequency	f_c	300	[kHz]
Bandwidth	Bw	75	[kHz]
Source Level	SL	179	[dB re μPa]
Absorption Coeff.	α	80	[dB/km]
Temperature	T	23	[°C]
Salinity	S	0	[ppt]
pH	pH	7	

The signals transmitted are 873.8 ms pseudo-noise (PN) sequences phase-modulated using Binary Phase Shift Keying (BPSK), pulse shaped using a conventional Root Raised Cosine (RRC) filter with a roll-off factor of 0.25 and transmitted between 262.5 kHz and 337.5 kHz (for a total bandwidth of 75 kHz). The different sources transmit different PN sequences. The resulting theoretical static channel impulse responses amplitudes $|h_{11}(\tau)|$, $|h_{12}(\tau)|$, $|h_{21}(\tau)|$ and $|h_{22}(\tau)|$ are presented in Figure 3.

The modeled channels generated using the method of images comprise a number of non-zero coefficients denoted $NZ_{11} = 71$, $NZ_{12} = 55$, $NZ_{21} = 55$ and $NZ_{22} = 71$ for each of $h_{11}(\tau)$, $h_{12}(\tau)$, $h_{21}(\tau)$, and $h_{22}(\tau)$ respectively [39].

B. RESULTS

1) TIME-INVARIANT MIMO CHANNEL AND CHOICE OF *P*

In this section, we compare the performance of the MIMO-OMP method and the trended-LS method in terms of their robustness to noise. We also study the impact of the number of iterations in the MIMO-OMP case. We apply both the trended-LS method and the MIMO-OMP method

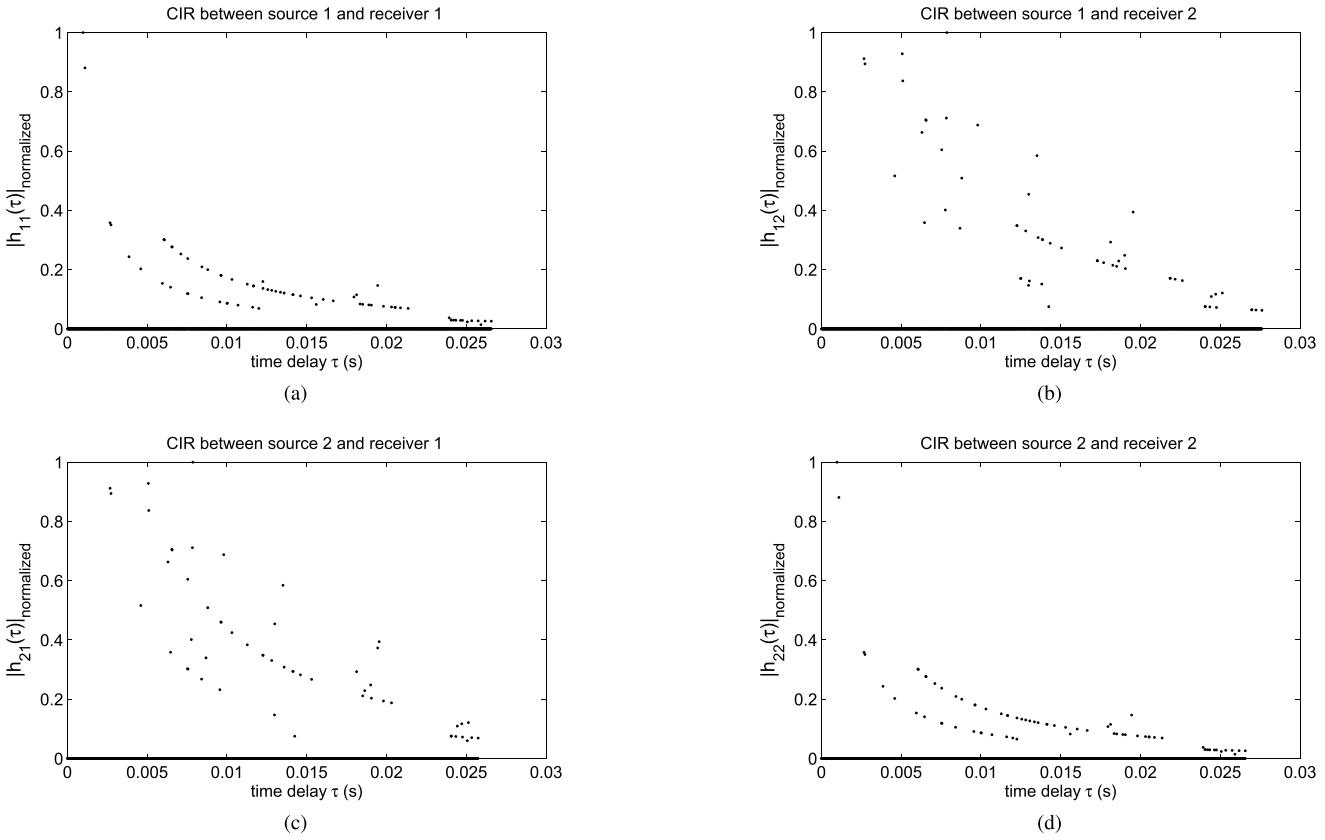

FIGURE 3. Modeled impulse responses $|h_{11}(\tau)|$, $|h_{12}(\tau)|$, $|h_{21}(\tau)|$ and $|h_{22}(\tau)|$.

to estimate the MIMO channel $h_{12}(\tau)$ modeled in Figure 3. We first analyze the performance of both algorithms as the ambient noise added to the signal increases. We assume that the ambient noise can be modeled as an Additive White Gaussian Noise (AWGN). Since the signal source level is constant, the study is performed as a function of the Signal-to-Noise Ratio (SNR). The number of iterations for the OMP method is adjustable. The simulation parameters for the channel estimation processes are presented in Table 2.

TABLE 2. Simulation parameters.

Parameters	Symbol	Value	
Window length for trended-LS estimation	L_w	4001	[samples]
Window length for MIMO-OMP estimation	L_w	2000	[samples]
Estimated channel length	L_c	2000	[samples]
Number of iterations for OMP	P	$1:100$	

The RMSE between the modeled channel, the trended-LS channel estimate and the MIMO-OMP channel estimate are shown in Figures 4 as a function of P for three SNR values (80 dB, 30 dB and 10 dB). Note that the trended-LS method is invariant with respect to P and varies only with respect to the SNR. As a reminder, we define the RMSE between a modeled CIR $h(\tau)$ and an estimated CIR $\hat{h}(\tau)$ as:

$$\text{RMSE} = \sqrt{\frac{\sum_{l=0}^{L_c-1}|h(\tau_l)-\hat{h}(\tau_l)|^2}{\sum_{l=0}^{L_c-1}|h(\tau_l)|^2}} \tag{7}$$

Figure 4 indicates that the trended-LS method becomes significantly less accurate than the MIMO-OMP method as the SNR drops. The apparent insensitivity of the MIMO-OMP to noise in estimating the echoes present in the channel comes from the fact that it only estimates the P most powerful echoes while assigning a zero value to the remaining echoes. As a result, the RMSE decreases as the number of iterations increases since the echoes are updated after every iteration. Moreover, an additional echo is estimated at every increment of P, resulting in a better channel estimation and a smaller RMSE between the modeled channel and the estimated channel. We conclude that the MIMO-OMP method estimation is much less sensitive to noise than the trended-LS method when the SNR varies between 10 and 80 dB. We also observe that at low SNR, the MIMO-OMP algorithm produces a smaller estimation error than the trended-LS estimation method does.

By analyzing the values of the RMSE as the number of iterations P in the MIMO-OMP method increases, we find that at first when $P \leq NZ$, as P increases, more non-zero echoes are estimated (so that less non-zero echoes are turned into nulls), while all null echoes are assigned a null value, therefore the RMSE decreases as P increases. When the number of iterations P is exactly equal to NZ, all non-zero echoes are estimated while all null echoes are assigned a null value, and the RMSE reaches its minimal value.

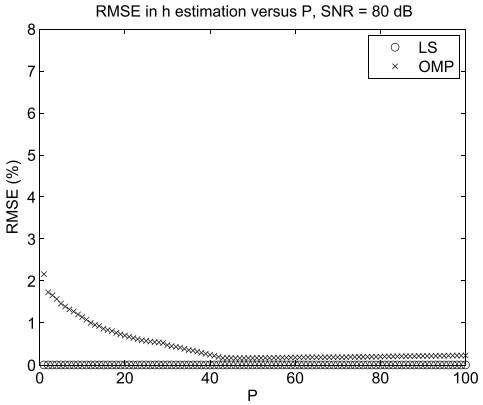

(a)

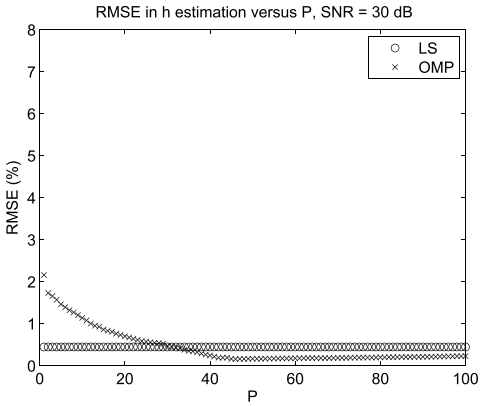

(b)

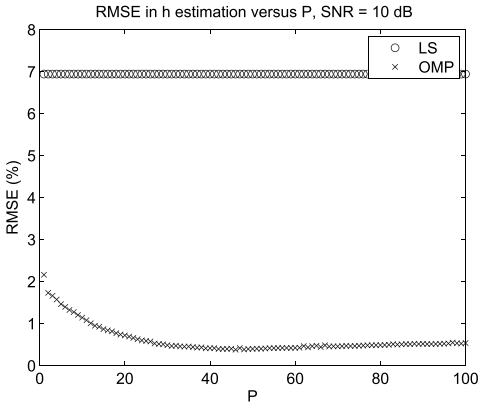

(c)

FIGURE 4. RMSE in estimating the time-invariant CIR, (a) SNR = 80 dB, (b) SNR = 30 dB, (c) SNR = 10 dB.

As P exceeds NZ, more null echoes are estimated instead of being automatically assigned a value of zero, causing the RMSE to slowly increase with P. Therefore, the optimal value for the number of iteration P in the MIMO-OMP case is exactly equal to the number of non-zero echoes present in the channel.

2) TIME-VARYING MIMO CHANNEL

We evaluate the performance of the proposed time-varying channel estimation algorithms by using the same modeled

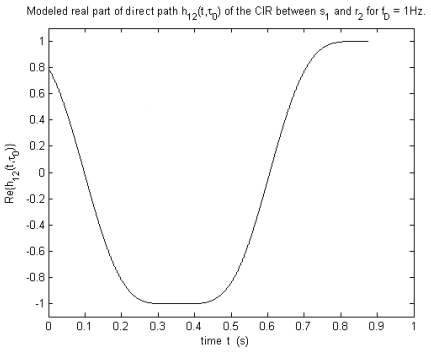

(a)

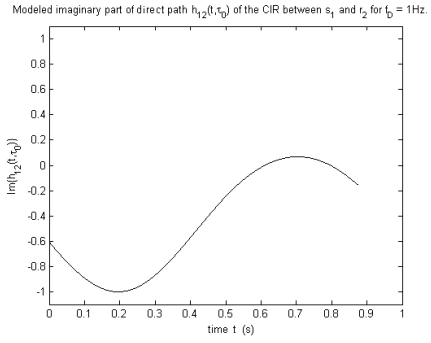

(b)

FIGURE 5. Time-varying model of the direct path $h_{12}(t, \tau_0)$ with $f_D = 1$ Hz. (a) Re$\{h_{12}(t, \tau_0)\}$, (b) Im$\{h_{12}(t, \tau_0)\}$.

static MIMO channel specified in Table 1. In the considered case of oscillating transducers, we introduce a sinusoidal Doppler spread $\Delta f(t)$ on each echo of maximum value f_D and angular frequency Ω such that [13]:

$$\Delta f(t) = f_D \cos(\Omega t). \tag{8}$$

We assign a maximum value $f_D = 1$ Hz with $\Omega = 6\pi$ rad/s and obtain a MIMO channel impulse response that is dependent both on time and on time delay. The signals transmitted at s_1 and s_2 are the same PN sequences used in the time-invariant case. The added noise corresponds to an SNR of 32 dB to match the experimental values presented in the next section. In this analysis, we present the time-variations of the direct path present in the channel $h_{12}(t, \tau)$ between s_1 and receiver r_2. The time variations of the channel's direct path, occurring at delay index $\text{ł}_0 = 74$, is denoted $h_{12}(t, \tau_0)$. The real and imaginary parts of this modeled echo are presented in Figure 5. In order to obtain a time-varying estimate of the CIR, we apply overlapping sliding windows of length $L_w = 2000$ (≈ 26.7 milliseconds). This short duration is chosen to ensure the stationarity of the channel within the observation window. The number of iteration for the MIMO-OMP algorithm is $P = 126$ to account for all non-zero echoes present in $h_{12}(t, \tau)$. Figure 6 shows the MIMO-OMP estimated real and imaginary parts of $h_{12}(t, \tau_0)$. Table 3 presents the RMSE between the time-varying model of the direct path $h_{12}(t, \tau_0)$

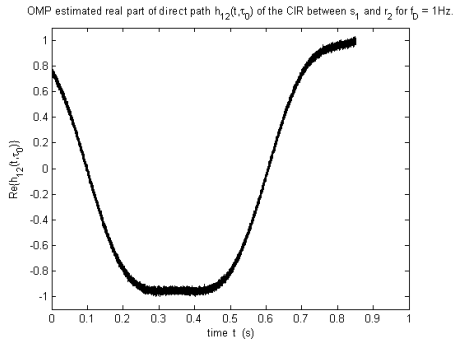

(a)

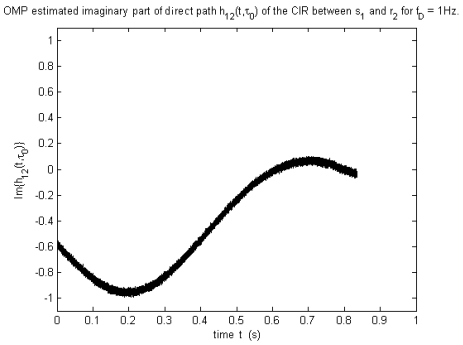

(b)

FIGURE 6. MIMO-OMP estimation of the direct path $h_{12}(t, \tau_0)$ with $f_D = 1$ Hz. (a) Re$\{h_{12}(t, \tau_0)\}$, (b) Im$\{h_{12}(t, \tau_0)\}$.

and its estimations using the LS, the trended-LS and the OMP-MIMO techniques.

TABLE 3. RMSE in $h_{12}(t, \tau_0)$ estimation using the LS, trended LS and MIMO-OMP methods.

Estimation Method	RMSE (%)
LS estimation	4.9
Trended-LS estimation	1.8
MIMO-OMP estimation	1.1

Table 3 clearly shows that at the given SNR, the MIMO-OMP method tracks more closely the time-variations in the CIR.

Next, we calculate the RMSE obtained for increasing values of added white Gaussian noise. We use five different AWGN for each SNR value of 0 B, 10 dB, 20 dB, and 32 dB. Figure 7 shows the RMSE achieved in each of the three methods as the SNR progresses from 0 dB to 32 dB. The plots are created using a 3^{rd}-order polynomial curve fitting.

Figure 7 also shows that the MIMO-OMP technique not only performs better than the Trended-LS and the LS techniques, but is also far less sensitive to the ambient noise, as it produces an almost constant RMSE for AWG noises of identical noise power density but with different time profiles, whereas the LS and the Trended-LS performances

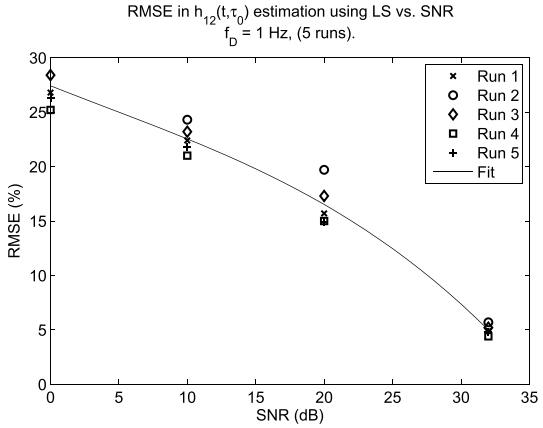

(a)

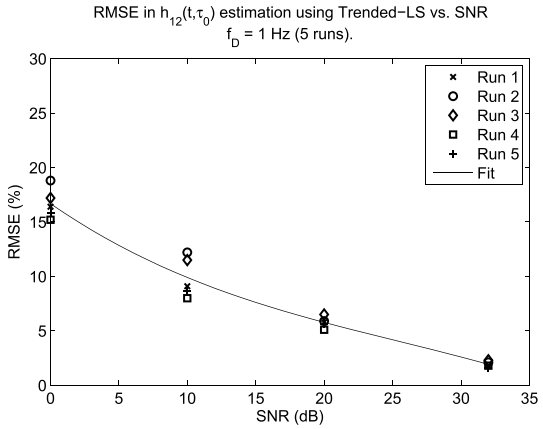

(b)

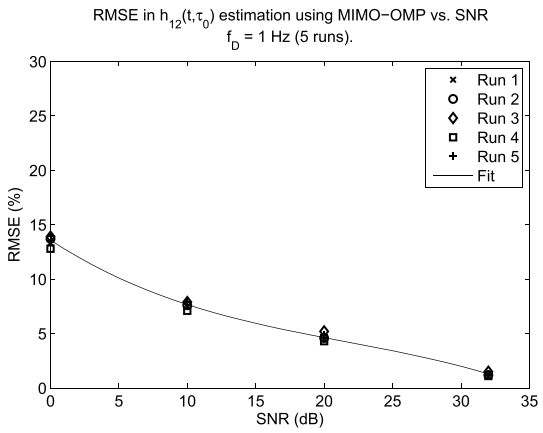

(c)

FIGURE 7. Simulation result of the RMSE vs. SNR for the estimated direct path between s_1 and r_2. (a) LS method. (b) Trended-LS method. (c) MIMO-OMP method.

fluctuate from one noise profile to the other. Therefore the MIMO-OMP technique is the most robust to AWG noise out of the three proposed algorithms. While both the Trended-LS and the MIMO-OMP methods perform better than the LS algorithm, the difference in performance between Trended-LS and MIMO-OMP is less pronounced. However, the execution time of the MIMO-OMP routine

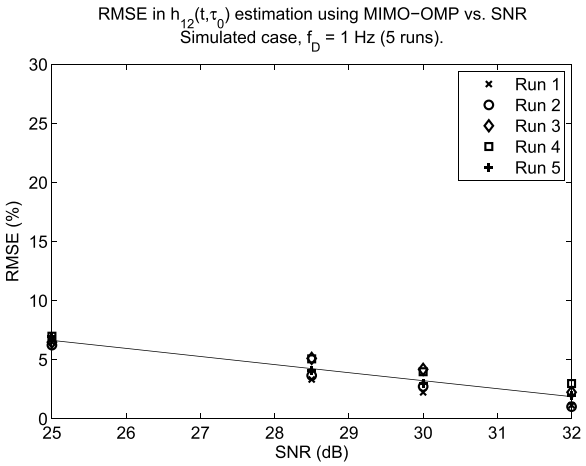

FIGURE 8. Simulation result of the RMSE vs. SNR for the estimated direct path between s_1 an r_2 using the MIMO-OMP method.

is much shorter than that of the Trended-LS for a similar performance.

Next, we run the same algorithm using SNR values that match those calculated in the experimental validation section: 25 dB, 28.5 dB, 30 dB and 32 dB. The results are plotted in Figure 8. Once again, the RMSE decreases as the SNR increases. This Figure is used for a comparative analysis in the experimental validation section.

Finally, we calculate the RMSE obtained for different values of the Doppler spread. We test three values: $f_D = 1, 10$ and 15 Hz and use five different AWG noises with a fixed SNR $= 32$ dB. The results are curve-fitted using a polynomial of order 3. The plots are shown in Figure 9.

We see that increasing values of Doppler spread cause the RMSE to increase significantly in the LS and Trended-LS cases, whereas the MIMO-OMP method provides steadier values. These results mark another advantage of the MIMO-OMP technique.

V. EXPERIMENTAL VALIDATION

A. SETUP

An experiment was conducted in the FAU outdoor test-pool and the sources' and receivers' placement was the same as in the simulation (Table 1). We use a broadband underwater acoustic source and receiver developed at Florida Atlantic University (FAU) [42]. The signals transmitted are identical to those used in the simulation (Cf. Section IV-A).

Controlling and reproducing the motion of sources and receivers is difficult. Therefore, we keep the transducers still and introduce the Doppler spread directly in the source signals. To do so, the source signals are modulated using a frequency $f_D = 1$ Hz to simulate slowly oscillating transducers and boundaries and obtain a channel estimate that depends both on time and time delay (time-varying MIMO channel). As in the simulation, the results presented are for the CIR between source s_1 and receiver r_2.

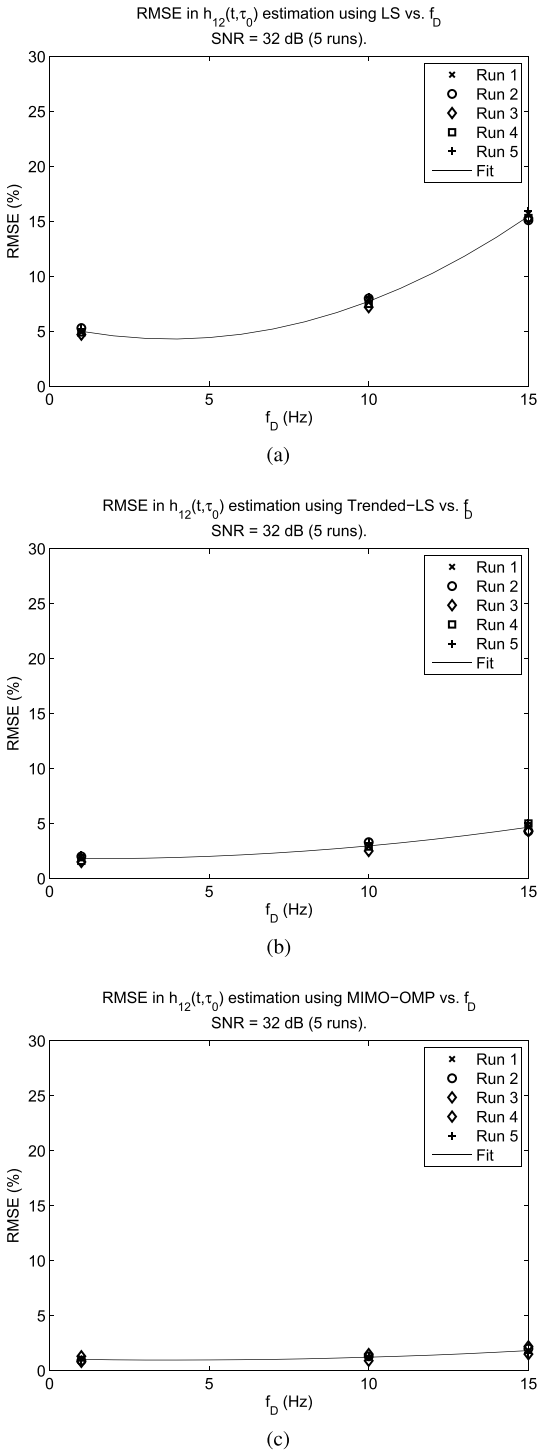

FIGURE 9. RMSE vs. Doppler spread for the estimated direct path between s_1 and r_2. (a) LS method. (b) Trended-LS method. (c) MIMO-OMP method.

B. RESULTS

The two sources s_1 and s_2 transmit simultaneously to r_1 and r_2. Without loss of generality, in our experimental analysis we present the results for the CIR between source s_1 and receiver r_2, namely $h_{12}(t, \tau)$. We note that the received signal

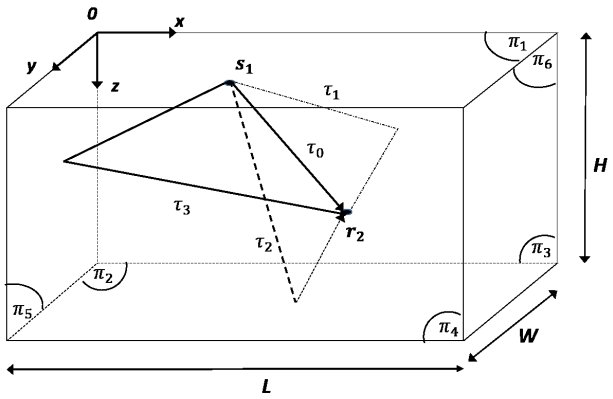

FIGURE 10. First four echoes between source s_1 and receiver r_2.

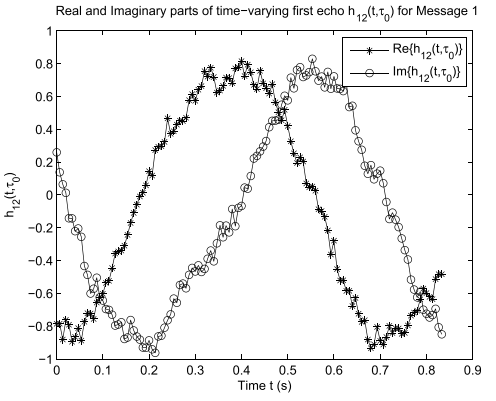

(a)

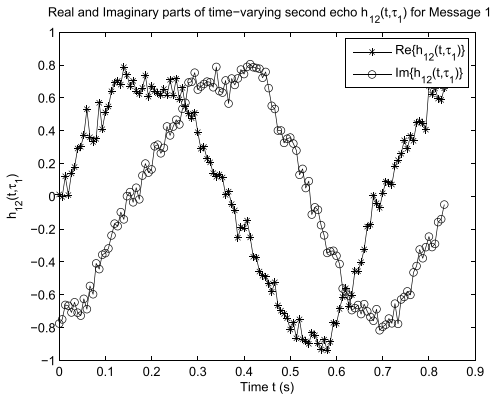

(b)

FIGURE 11. MIMO-OMP estimate of normalized real and imaginary parts, Message 1. (a) $h_{12}(t, \tau_0)$, (b) $h_{12}(t, \tau_1)$.

at r_2 comes from both s_1 and s_2. We focus the analysis on the direct path of the CIR between s_1 and r_2, namely $h_{12}(t, \tau_0)$, and on the first three echoes that each bounce off one of the pool walls Π_2, Π_3 and Π_5. The corresponding propagation times are τ_0, τ_1, τ_2 and τ_3. The source and the receiver are placed respectively at coordinates $(W/4, L/4, 0.1)$ and $(3W/4, L/2, 1.6)$. Because of the pool dimensions (Figure 10), the two transducers are closer to the side wall Π_3 and the bottom Π_2 than to the front walls Π_5, which produces very close values for τ_1,τ_2.

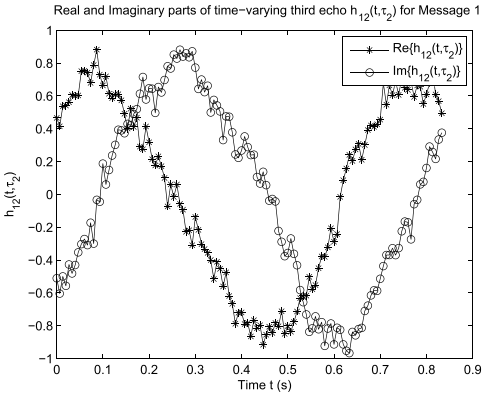

(a)

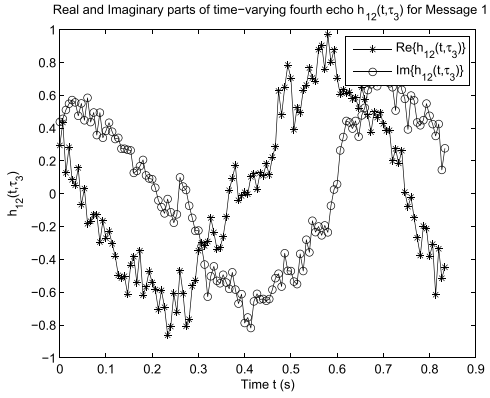

(b)

FIGURE 12. MIMO-OMP estimate of normalized real and imaginary parts, Message 1. (a) $h_{12}(t, \tau_2)$, (b) $h_{12}(t, \tau_3)$.

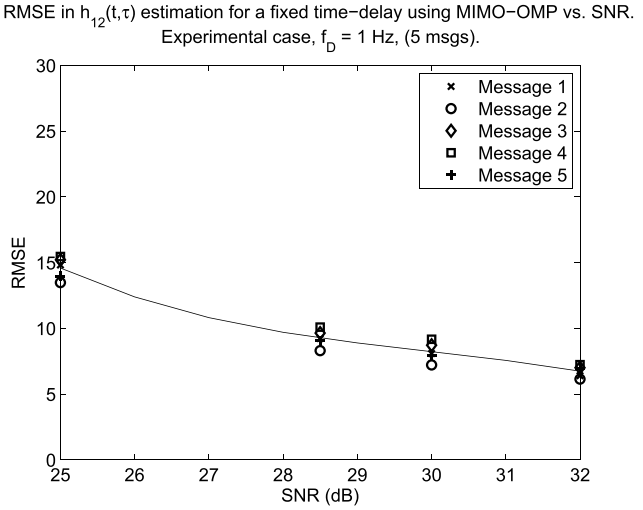

FIGURE 13. RMSE vs. SNR between s_1 and r_2 at a fixed time-delay using the MIMO-OMP method and experimental data. The SNR is calculated according to equation (8).

Next, we calculate the RMSE obtained for increasing values of SNR. The signal associated with the direct path is received with an SNR of 32 dB. The SNR for every subsequent path is computed as a function of the SNR of the

direct path. For each path l, the SNR is calculated as:

$$\mathrm{SNR}_l = 32 + 10\log_{10}\left(\frac{\sigma^2_{h_{12}(t,\tau_l)}}{\sigma^2_{h_{12}(t,\tau_0)}}\right) \quad [\mathrm{dB}] \qquad (9)$$

where $\sigma^2_{h_{12}(t,\tau_l)}$ represents the variance of $h_{12}(t,\tau_l)$. As in the simulation section, we base our analysis on five different messages. To keep the paper concise, we only show the time-varying estimated echoes for message 1 in Figures 11 and 12. Figure 13 shows the resulting RMSE vs. SNR plot for Messages 1 to 5. This plot is created using a 3^{rd}-degree polynomial curve fitting.

We observe in Figures 11 and 12 that the MIMO-OMP method yields results that clearly show the expected time fluctuation of the four echoes.

We notice by comparing Figure 8 and Figure 13 that the results in the experimental part are close to the values obtained in simulation. The estimation error is smaller in simulation for the following reasons: (1) Inaccuracies in the transducers placement in the experiment as it was not exactly matching the simulation values; (2) Inaccuracies in the estimation due to the presence of multiple echoes arriving at very similar time of arrival.

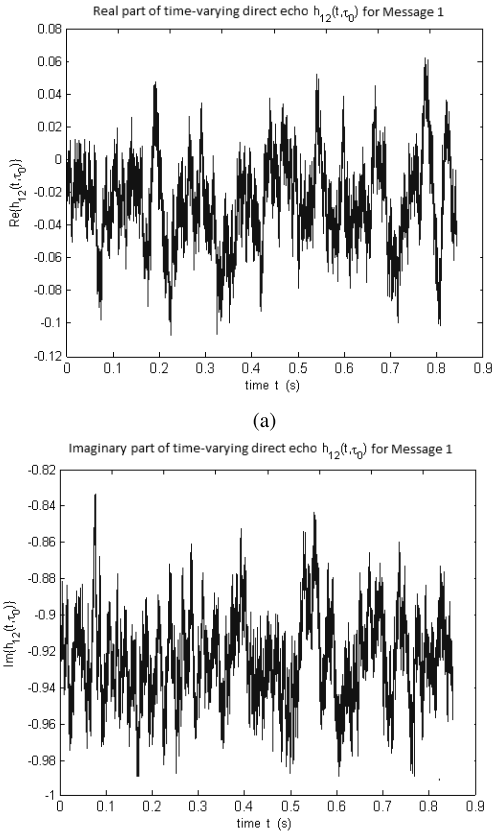

FIGURE 14. Trended-LS estimate of $h_{12}(t,\tau_0)$, Message 1. (a) Real part, (b) Imaginary part.

By contrast, Figures 14a and 14b show the real and imaginary parts of the estimated CIR direct path at time delay $\tau = \tau_0$ as a function of time obtained using the trended-LS approach. Since the results for the direct path are already so noisy, we do not show the results for the subsequent echoes. Clearly, we can conclude that the MIMO-OMP technique performs much better that the trended-LS technique when applied to real data and is therefore a better choice for high frequency MIMO channel estimation.

VI. CONCLUSION

This paper sought to address one of the challenges posed by the underwater acoustic channel, namely finding a robust channel estimation technique that closely tracks the time variations of the echoes forming the MIMO channel impulse response at very-high frequencies. We have proposed and evaluated the performance of the suggested MIMO-OMP algorithm on simulated data as well as on experimental results. We first analyzed the use of the CIR estimation techniques with time-invariant channels to show the optimal choice for the number of iterations. We compared the algorithm to both the LS and the trended-LS technique, and the results obtained have shown that the MIMO-OMP algorithm is the most robust with respect to added noise.

In a second set of simulations, we modeled time-varying MIMO channels with various values of Doppler spread. One of the most interesting results in this respect is the performance of the MIMO-OMP algorithm as the Doppler spread f_D increases: it is observed that the MIMO-OMP method provides steady values of RMSE as f_D varies, in strong contrast to both the LS and trended-LS techniques where the RMSE increases significantly as the Doppler spread increases.

In analyzing the time variations of four specific paths for estimated MIMO channels, the experimental data clearly showed that the MIMO-OMP technique was able to track the time-variations in the channel even as the SNR decreased. In addition, it was demonstrated that the MIMO-OMP algorithm remained robust in terms of achieved RMSE in time-varying case as the SNR varied, matching in that aspect the simulation results. A potential improvement on this approach is to further exploit the sparsity of the underwater acoustic channel by considering its delay Doppler spread function, as proposed in [15], and apply it to MIMO configurations.

REFERENCES

[1] J. A. Catipovic *et al.*, "Performance limitations in underwater acoustic telemetry," *IEEE J. Ocean. Eng.*, vol. 15, no. 3, pp. 205–216, Jul. 1990.
[2] M. Stojanovic, J. Catipovic, and J. G. Proakis, "Adaptive multichannel combining and equalization for underwater acoustic communications," *J. Acoust. Soc. Amer.*, vol. 94, no. 3, pp. 1621–1631, Sep. 1993.
[3] M. Stojanovic, "Acoustic (Underwater) Communications," in *Encyclopedia of Telecommunications*. New York, NY, USA: Wiley, 2003.
[4] I. Iturbe, P. Roux, B. Nicolas, J. Virieux, and J. I. Mars, "Shallow-water acoustic tomography performed from a double-beamforming algorithm: Simulation results," *IEEE J. Ocean. Eng.*, vol. 34, no. 2, pp. 140–149, Apr. 2009.

[5] F. Aulanier, B. Nicolas, J. I. Mars, P. Roux, and R. Brossier, "Shallow-water acoustic tomography from angle measurements instead of travel-time measurements," *J. Acoust. Soc. Amer.*, vol. 134, no. 4, pp. EL373–EL379, 2013.

[6] P. Roux, I. Iturbe, B. Nicolas, J. Virieux, and J. I. Mars, "Travel-time tomography in shallow water: Experimental demonstration at an ultrasonic scale," *J. Acoust. Soc. Amer.*, vol. 130, no. 3, pp. 1232–1241, 2011.

[7] W. Munk and C. Wunsch, "Ocean acoustic tomography: A scheme for large scale monitoring," *Deep Sea Res. A, Oceanogr. Res. Papers*, vol. 26, no. 2, pp. 123–161, 1979.

[8] B. Cornuelle *et al.*, "Tomographic maps of the ocean mesoscale. Part 1: Pure acoustics," *J. Phys. Oceanogr.*, vol. 15, no. 2, pp. 133–152, 1985.

[9] P. F. Worcester, R. C. Spindel, and B. M. Howe, "Reciprocal acoustic transmissions: Instrumentation for mesoscale monitoring of ocean currents," *IEEE J. Ocean. Eng.*, vol. OE-10, no. 2, pp. 123–137, Apr. 1985.

[10] N. Taniguchi *et al.*, "Long-term acoustic tomography measurement of ocean currents at the northern part of the Luzon strait," *Geophys. Res. Lett.*, vol. 37, no. 7, p. L07601, 2010.

[11] W. Munk, P. Worcester, and C. Wunsch, *Ocean Acoustic Tomography*. Cambridge, U.K.: Cambridge Univ. Press, 2009.

[12] I. F. Akyildiz, D. Pompili, and T. Melodia, "Underwater acoustic sensor networks: Research challenges," *Ad Hoc Netw.*, vol. 3, no. 3, pp. 257–279, Mar. 2005.

[13] S. Kaddouri, P.-P. J. Beaujean, P.-J. Bouvet, and G. Real, "Least square and trended doppler estimation in fading channel for high-frequency underwater acoustic communications," *IEEE J. Ocean. Eng.*, vol. 39, no. 1, pp. 179–188, Jan. 2014.

[14] S. Kaddouri, P.-P. Beaujean, and P.-J. Bouvet, "Doppler estimation in fading channel for high frequency underwater acoustic communication," in *Proc. IEEE UComms*, Sestri Levante, Italy, Sep. 2012, pp. 1–7.

[15] W. Li and J. C. Preisig, "Estimation of rapidly time-varying sparse channels," *IEEE J. Ocean. Eng.*, vol. 32, no. 4, pp. 927–939, Oct. 2007.

[16] C. R. Berger, Z. Wang, J. Huang, and S. Zhou, "Application of compressive sensing to sparse channel estimation," *IEEE Commun. Mag.*, vol. 48, no. 11, pp. 164–174, Nov. 2010.

[17] T. Kang and R. A. Iltis, "Iterative carrier frequency offset and channel estimation for underwater acoustic OFDM systems," *IEEE J. Sel. Areas Commun.*, vol. 26, no. 9, pp. 1650–1661, Dec. 2008.

[18] M. Stojanovic, "OFDM for underwater acoustic communications: Adaptive synchronization and sparse channel estimation," in *Proc. IEEE Int. Conf. Acoust., Speech Signal Process. (ICASSP)*, Mar./Apr. 2008, pp. 5288–5291.

[19] C. R. Benson and M. R. Frater, "High data rates in the high frequency acoustic channel," in *Proc. MTS/IEEE Washington OCEANS*, Oct. 2015, pp. 1–4.

[20] S. Roy, T. M. Duman, V. McDonald, and J. G. Proakis, "High-rate communication for underwater acoustic channels using multiple transmitters and space–time coding: Receiver structures and experimental results," *IEEE J. Ocean. Eng.*, vol. 32, no. 3, pp. 663–688, Jul. 2007.

[21] P. Flandrin, "An empirical model for electronic submissions to conferences," *Adv. Complex Syst.*, vol. 13, no. 3, pp. 439–449, 2010.

[22] L. M. Brekhovskikh and Y. P. Lysanov, *Fundamentals of Ocean Acoustics*. New York, NY, USA: Springer, 2003.

[23] Z. Yang and Y. R. Zheng, "Iterative channel estimation and turbo equalization for multiple-input multiple-output underwater acoustic communications," *IEEE J. Ocean. Eng.*, vol. 41, no. 1, pp. 232–242, Jan. 2016.

[24] B. Paradis, C. L. Bachand, P. J. Gendron, and D. A. Brown, "Development of a high frequency underwater acoustic communication modem," in *Proc. Meetings Acoust. (ASA)*, 2014, vol. 21. no. 1, p. 055006.

[25] A. Zhang, S. Yang, and G. Gui, "Sparse channel estimation for MIMO-OFDM two-way relay network with compressed sensing," *Int. J. Antennas Propag.*, vol. 2013, Feb. 2013, Art. no. 914734.

[26] Y. Peng, X. Yang, X. Zhang, W. Wang, and B. Wu, "Compressed MIMO-OFDM channel estimation," in *Proc. 12th IEEE Int. Conf. Commun. Technol. (ICCT)*, Nov. 2010, pp. 1291–1294.

[27] G. Gui, Q. Wan, W. Peng, and F. Adachi. (May 2010). "Sparse multipath channel estimation using compressive sampling matching pursuit algorithm." [Online]. Available: https://arxiv.org/abs/1005.2270

[28] G. Real, P.-P. Beaujean, and P.-J. Bouvet, "MIMO underwater acoustic communications in ports and shallow waters at very high frequency," *J. Sens. Actuator Netw.*, vol. 2, no. 4, pp. 700–716, 2013.

[29] M. Kocic, D. Brady, and M. Stojanovic, "Sparse equalization for real-time digital underwater acoustic communications," in *Proc. MTS/IEEE Challenges Changing Global Environ. Conf. (OCEANS)*, vol. 3. Oct. 1995, pp. 1417–1422.

[30] C. R. Berger, S. Zhou, J. C. Preisig, and P. Willett, "Sparse channel estimation for multicarrier underwater acoustic communication: From subspace methods to compressed sensing," *IEEE Trans. Signal Process.*, vol. 58, no. 3, pp. 1708–1721, Mar. 2010.

[31] J. Huang, C. R. Berger, S. Zhou, and J. Huang, "Comparison of basis pursuit algorithms for sparse channel estimation in underwater acoustic OFDM," in *Proc. IEEE-Sydney OCEANS*, May 2010, pp. 1–6.

[32] C. Qi, X. Wang, and L. Wu, "Underwater acoustic channel estimation based on sparse recovery algorithms," *IET Signal Process.*, vol. 5, no. 8, pp. 739–747, 2011.

[33] S. F. Cotter and B. D. Rao, "Matching pursuit based decision-feedback equalizers," in *Proc. IEEE Int. Conf. Acoust., Speech, Signal Process. (ICASSP)*, vol. 5. Jun. 2000, pp. 2713–2716.

[34] S. F. Cotter and B. D. Rao, "Sparse channel estimation via matching pursuit with application to equalization," *IEEE Trans. Commun.*, vol. 50, no. 3, pp. 374–377, Mar. 2002.

[35] A. M. Bruckstein, D. L. Donoho, and M. Elad, "From sparse solutions of systems of equations to sparse modeling of signals and images," *SIAM Rev.*, vol. 51, no. 1, pp. 34–81, 2009.

[36] G. Z. Karabulut and A. Yongacoglu, "Sparse channel estimation using orthogonal matching pursuit algorithm," in *Proc. IEEE 60th Veh. Technol. Conf. (VTC-Fall)*, vol. 6. Sep. 2004, pp. 3880–3884.

[37] B. D. Rao, "Signal processing with the sparseness constraint," in *Proc. IEEE Int. Conf. Acoust., Speech Signal Process.*, vol. 3. May 1998, pp. 1861–1864.

[38] E. Vlachos, A. S. Lalos, and K. Berberidis, "Stochastic gradient pursuit for adaptive equalization of sparse multipath channels," *IEEE J. Emerg. Sel. Topics Circuits Syst.*, vol. 2, no. 3, pp. 413–423, Sep. 2012.

[39] S. Kaddouri, P.-J. Bouvet, and P.-P. Beaujean, "Sparse channel estimation for time-varying MIMO underwater acoustic channels at very-high frequencies," in *Proc. ACM Int. Conf. Underwater Netw. Syst.*, 2014, p. 35.

[40] S. Kaddouri, "Underwater acoustic channel estimation using multiple sources and receivers in shallow waters at very-high frequencies," Ph.D. dissertation, College Eng. Comput. Sci., Florida Atlantic Univ., Boca Raton, FL, USA, 2015.

[41] P.-P. J. Beaujean and M. D. Staska, "High-frequency underwater acoustic propagation in a port modeled as a three-dimensional duct closed at one end using the method of images," *Adv. Acoust. Vibrat.*, vol. 2012, Apr. 2012, Art. no. 929174.

[42] P.-P. J. Beaujean and E. A. Carlson, "HERMES—A high bit-rate underwater acoustic modem operating at high frequencies for ports and shallow water applications," *Marine Technol. Soc. J.*, vol. 43, no. 2, pp. 21–32, 2009.

SAMAR KADDOURI (M'12) received the M.S. degree in electrical and computer engineering from the Georgia Institute of Technology, Atlanta, GA, USA, and the Ph.D. degree in ocean engineering from Florida Atlantic University in 2011 and 2015, respectively. She was a Fulbright Science and Technology Fellow with the Georgia Institute of Technology.

In 2016, she joined the National Institute of Applied Science, Rennes, France. Her current research interests include underwater acoustic communications, underwater networks, multi-in multi-out transmission, and 5G communications.

PIERRE-PHILIPPE J. BEAUJEAN (M'01) received the Ph.D. degree in ocean engineering from Florida Atlantic University in 2001. He is currently a Professor with the Department of Ocean and Mechanical Engineering, Florida Atlantic University. He specializes in the field of underwater acoustics, signal processing, sonar design, data analysis, machine health monitoring, and vibrations control. He is an active member of the Acoustical Society of America.

PIERRE-JEAN BOUVET (M'10) was born in Clermont-Ferrand, France, in 1978. He received the Dipl.-Ing. and Ph.D. degrees in electrical engineering from the National Institute of Applied Science, Rennes, France, in 2001 and 2005, respectively.

In 2005, he joined NXP Semiconductors, Caen, France, as a Baseband Decoding Architect for digital TV demodulator products (DVB-T/T2). Since 2009, he has been an Associate Professor with the Department of Embedded Systems, Acoustic and Communications, ISEN, Brest, France. His current research interests include underwater acoustic communications, underwater network, multi-in multi-out transmission, iterative reception, synchronization, and localization algorithms.